Proceedings of the LHCP2015 Conference, St. Petersburg, Russia, August 31 - September 5, 2015

Editors: V.T. Kim and D.E. Sosnov

Vector boson production at the LHC: transverse-momentum resummation and leptonic decay

GIANCARLO FERRERA

Dipartimento di Fisica, Università di Milano and INFN, Sezione di Milano, I-20133 Milan, Italy.

giancarlo.ferrera@mi.infn.it

Abstract. We present results for the transverse-momentum (q_T) distribution of W and Z/γ^* bosons produced in hadronic collisions. At small value of q_T, the logarithmically-enhanced perturbative QCD contributions are resummed up to next-to-next-to-leading logarithmic accuracy. Resummed results are consistently combined with the complete $O(\alpha_S^2)$ fixed-order result at small, intermediate and large values of q_T. The leptonic decay of the vector boson is explicitly included with the corresponding spin correlations, the finite-width effects and the full dependence on the final-state lepton(s) kinematics. The recoil due to the transverse momentum of the vector boson is consistently and explicitly treated in the resummed calculation. We present a comparison of some of the available LHC data with the results obtained with the numerical program `DYRes`, which allows the user to apply arbitrary kinematical cuts on the final-state leptons and to compute the corresponding distributions in the form of bin histograms.

Introduction

The production of W and Z/γ^* bosons in hadronic collisions, through the Drell–Yan (DY) mechanism [1], is a process of great importance for physics studies within and beyond the Standard Model.

Accurate theoretical predictions for the DY production cross section and related kinematical distributions require the evaluation of QCD radiative corrections. The total cross section [2] and the rapidity distribution [3] of the vector boson are known up to the next-to-next-to-leading order (NNLO). Two independent fully differential NNLO calculations, which include the leptonic decay of the vector boson, have been performed [4, 5, 6]. Electroweak (EW) [7] and mixed QCD-EW [8] corrections have also been considered.

An observable which is particularly relevant is the vector boson transverse-momentum (q_T). In the region of large q_T ($q_T \sim m_V$, where m_V is the vector boson mass), fixed-order QCD corrections are known analytically up to $O(\alpha_S^2)$ [9, 10, 11, 12, 13] and numerically at $O(\alpha_S^3)$ [14, 15].

Nonetheless the bulk of the vector boson cross section lies in the small-q_T region ($q_T \ll m_V$), where the reliability of the fixed-order expansion is spoiled by the presence of large logarithmic corrections, $\alpha_S^n\ (m_V^2/q_T^2)\ln^m(m_V^2/q_T^2)$ (with $0 \le m \le 2n-1$), due to soft and collinear parton emissions. The reliability of perturbation theory at small q_T can be restored by resumming these logarithmically-enhanced terms to all orders [16]–[25]. Resummed and fixed-order calculations can be consistently matched to achieve a uniform accuracy from small to large values of q_T.

The resummed calculation up to next-to-next-to-leading logarithmic (NNLL) accuracy performed in Refs. [26, 27] have been extended in Ref. [28] to W and Z/γ^* boson. Moreover in Ref. [28] the leptonic decay of the vector boson with the corresponding spin correlations has been explicitly included [1].

The inclusion of the vector boson leptonic decay is particularly important because hadron collider experiments can directly measure only the decay products of vector bosons in finite kinematical regions. By retaining the kinematics of the final-state leptons it is possible to apply in the theoretical calculation the kinematical selection cuts of the corresponding experimental analyses.

The spin of the vector boson dynamically correlates the decaying lepton momenta with the transverse momentum acquired by the vector boson through its production mechanism. Through the resummation procedure at fixed lepton momenta, higher-order contributions due to soft and collinear multiparton radiation dynamically produce a finite value

[1] A detailed discussion of the resummation formalism we have employed can be found in Refs. [21, 22, 23, 25]

of the transverse momentum q_T of the lepton pair which, once distributed between the lepton momenta, affects the lepton angular distribution. This q_T-recoil effect is a non-singular contribution to the q_T cross section at small values of q_T and, therefore, cannot be unambiguously computed through the transverse-momentum resummation formalism. Therefore the inclusion of the full dependence on the lepton decay variables in the resummed calculation requires the implementation of a q_T-recoil prescription [2].

The vector boson computation of Ref. [28] is implemented in the numerical code `DYRes`, which allows the user to apply arbitrary kinematical cuts on the final-state leptons and to compute the corresponding relevant distributions in the form of bin histograms [3]. The code `DYRes` is publicly available and it can be downloaded from the URL address `http://pcteserver.mi.infn.it/~ferrera/dyres.html` .

Numerical results at the LHC

We consider the processes $pp \to Z/\gamma^* \to l^+l^-$ and $pp \to W^\pm \to l\nu_l$ at LHC energies. We present our resummed results at NNLL+NNLO and NLL+NLO accuracy [4], and we compare them with some of the available LHC data. The hadronic cross sections is computed by using the NNPDF3.0 [37] parton densities functions (PDFs) with $\alpha_S(m_Z^2) = 0.118$. The input electroweak parameters in the G_μ scheme (G_F, m_Z, m_W) are taken from the PDG 2014 [38].

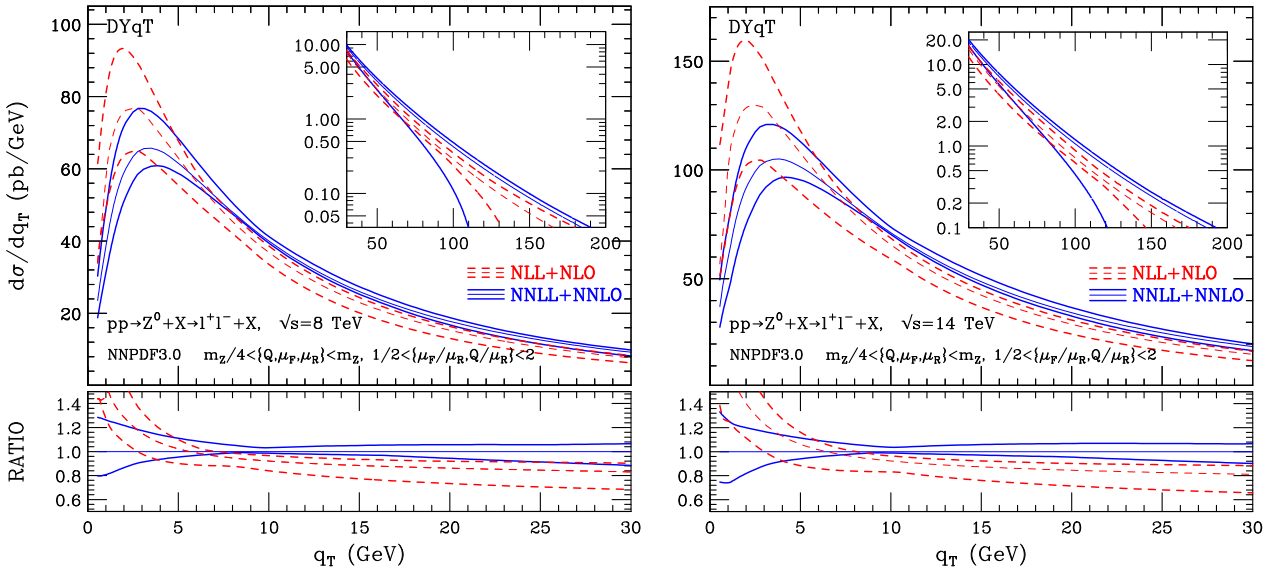

FIGURE 1. NLL+NLO (red dashed) and NNLL+NNLO (blue solid) results for the q_T spectrum of Z bosons at the LHC with energies $\sqrt{s}$ =8 TeV (left panel) and $\sqrt{s}$ =14 TeV (right panel). The lower panel presents the ratio of the scale-dependent NLL+NLO and NNLL+NNLO results with respect to the NNLL+NNLO result at the central value of the scales.

We start the presentation from the inclusive results for the q_T spectrum. The numerical results are obtained by using the `DYqT` code [26, 27] [5].

The NLL+NLO and NNLL+NNLO results for the q_T spectrum of on-shell Z boson produced at the LHC with $\sqrt{s}$ =8 TeV and $\sqrt{s}$ =14 TeV are presented in Fig. 1. At each logarithmic accuracy we present the result at the central value factorization, renormalization and resummation [39] scales, $\mu_F = \mu_R = Q = m_Z/2$, and a corresponding uncertainty band obtained through independent variations of μ_F, μ_R and Q in the range $m_Z/4 \le \{\mu_F, \mu_R, Q\} \le m_Z$ with the constraints $0.5 \le \mu_F/\mu_R \le 2$ and $0.5 \le Q/\mu_R \le 2$. The lower panels in Fig. 1 present the ratio of the

[2] A general and consistent procedure that is directly applicable to q_T resummed calculations for generic production processes of high-mass systems in hadron collisions has been introduced and discussed in Ref. [28].

[3] Analogous calculations were performed for Higgs boson [35] and diboson production [36].

[4] The label NNLO (NLO) refers to the fixed-order perturbative accuracy in the small-q_T region and for the total cross section, the corresponding perturbative accuracy in the large-q_T region is NLO (LO).

[5] The code `DYqT` is publicly available and it can be downloaded from `http://pcteserver.mi.infn.it/~ferrera/dyqt.html` .

scale-dependent NLL+NLO and NNLL+NNLO results with respect to the NNLL+NNLO result at the central value $\mu_F = \mu_R = Q = m_Z/2$ of the scales.

The region of small and intermediate values of q_T is shown in the main panels of Fig. 1. At fixed centre–of–mass energy the NNLL+NNLO q_T spectrum is harder than the spectrum at NLL+NLO accuracy. At fixed value of q_T the cross section sizeably increases by increasing the centre–of–mass energy from 8 TeV to 14 TeV. The shape of the NNLL+NNLO q_T spectrum is slightly harder at the higher energy. The NLL+NLO scale-variation band is wider than the NNLL+NNLO band. The NLL+NLO and NNLL+NNLO bands overlap at small transverse momenta and remain very close by increasing q_T. The NNLL+NNLO (NLL+NLO) scale dependence is about ±10% (±20%) at the peak, it decreases to about ±2% (±7%) at $q_T \simeq 10$ GeV and increases to about ±6% (±10%) at $q_T \sim 25$ GeV.

The inset plots show the cross section in the large-q_T region. The resummation results obtained with DYqT and reported in the inset plots are presented for illustrative purposes. At large values of q_T ($q_T \gtrsim m_Z$) the resummed result looses predictivity, and its perturbative uncertainty becomes large. In this region the resummation cannot improve the predictivity of fixed-order calculations and the resummed result has to be replaced by the standard fixed-order prediction.

We have estimated the non perturbative (NP) effects, related to the intrinsic transverse-momentum of partons inside the colliding hadrons, with a simple model which include a free parameter and we have studied the uncertainties related to the parton distribution functions (PDFs). In summary, from our brief analysis on the possible impact of NP effects for vector boson production at the LHC, we conclude that our conservative) estimate leads to quantitative effects that are small and well within the perturbative scale variation dependence, still in the very low q_T region. A quantitatively similar conclusion applies to the effect of PDF uncertainties. Based on these observations we limit ourselves to considering only the perturbative calculation and the corresponding scale variation uncertainties.

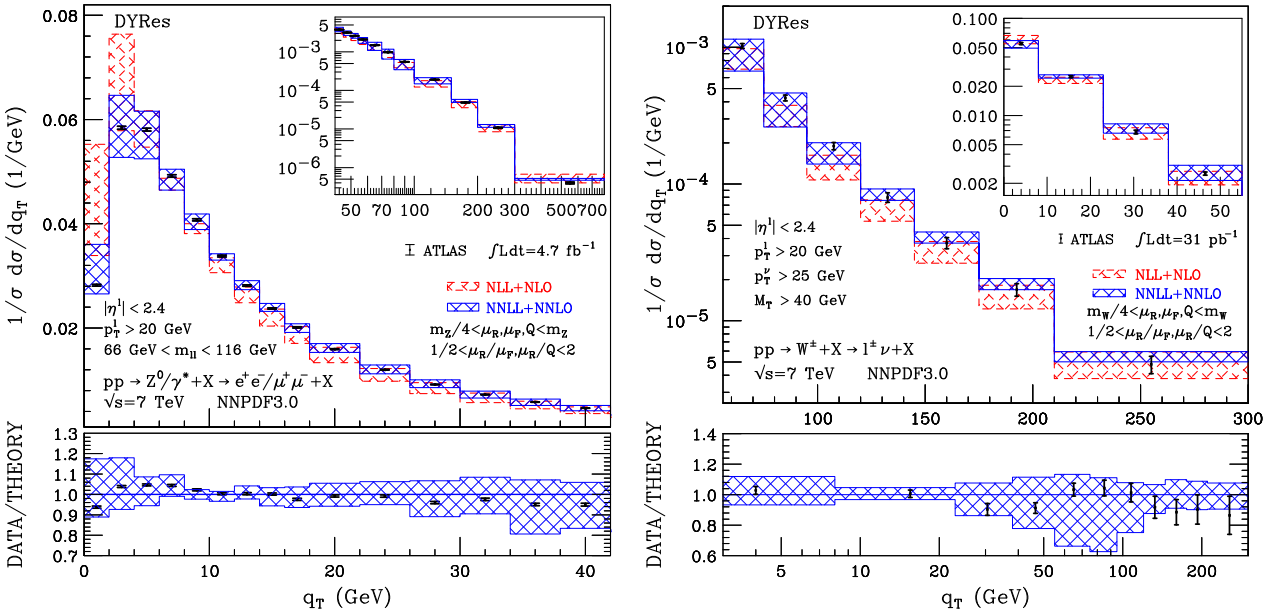

FIGURE 2. Vector boson production at the LHC with lepton selection cuts. The NLL+NLO (red) and NNLL+NNLO (blue) normalized q_T spectra compared with the ATLAS data: Z/γ^* production [40] (left panel) and $W^\pm$ production [42] (right panel). The inset plot shows the ratio of the data and of the scale dependent NNLL+NNLO result with respect to the NNLL+NNLO result at central values of the scales.

We now consider the measurement of the q_T spectrum of dilepton pairs at the LHC with $\sqrt{s} = 7$ TeV, as reported by the ATLAS [40] Collaboration with an integrated luminosity of 4.7 fb^{-1} [6]. The cuts that define the fiducial region in which the measurement is performed (our corresponding calculation is carried out in the same region) are as follows. The invariant mass m_{ll} of the lepton pair is required to be in the range 66 GeV $< m_{ll} <$ 116 GeV, and the leptons must

[6] An analogous measurement of the q_T distribution at the LHC was reported by the CMS Collaboration [41] with a smaller integrated luminosity of 36 pb^{-1}.

be in the central rapidity region, with pseudorapidity $|\eta^l| < 2.4$, and they have a transverse momentum $p_T^l > 20$ GeV.

The results of our resummed calculation are shown in Fig. 2 (a). The blue-solid (red-dashed) histogram is the NNLL+NNLO (NLL+NLO) prediction for the q_T spectrum, which is normalized to the cross section in the fiducial region, and the points are the data with the corresponding experimental errors. The inset plot shows the high-q_T region while the lower panel shows the data and the scale dependent NNLL+NNLO prediction normalized to the NNLL+NNLO result at central values of the scales ($\mu_F = \mu_R = Q = m_Z/2$). The scale dependence band of the perturbative calculation is computed by varying μ_F, μ_R and Q as previously discussed. We see that our perturbative calculation is consistent with the data within the uncertainties and that the scale variation bands at NLL+NLO and NNLL+NNLO accuracy overlap. Moreover, in going from NLL+NLO to NNLL+NNLO accuracy the perturbative uncertainty is reduced and the agreement between experimental data and theory prediction is improved. The perturbative uncertainty at NNLL+NNLO accuracy is about ±10% at the peak, it decreases to about ±4% at $q_T \sim 10$ GeV, and it increases again to about ±10% at $q_T = 40$ GeV.

In Fig. 2 (b) we consider the q_T spectrum of $W^\pm$ bosons. We present a comparison of our resummed results with the $pp \to W \to l\nu$ data collected by the ATLAS Collaboration [42] with an integrated luminosity of 31 pb^{-1} at $\sqrt{s} = 7$ TeV. The fiducial region is defined as follows: the charged lepton has transverse momentum $p_T^l > 20$ GeV and pseudorapidity $|\eta^l| < 2.4$, the missing transverse energy is $p_T^\nu > 25$ GeV, and transverse mass $m_T = \sqrt{2p_T^l\, p_T^\nu(1-\cos(\phi^l - \phi^\nu))}$ is constrained in the region $m_T > 40$ GeV. In the small q_T region, the bin sizes of the experimental data are rather large and in Fig. 2 (b) we focus on the large q_T region 55 GeV $< q_T <$ 300 GeV (the small q_T region is shown in the inset plot). The lower panel of Fig. 2 (b) presents the ratio of both data and theoretical results with respect to the reference theoretical result. The ratio and the scale variation bands are computed as in the case of Fig. 2. We see that our NNLL+NNLO calculation describes the W production data within the perturbative uncertainties. The NNLL+NNLO perturbative uncertainty is about ±8% at the peak, it decreases to about ±4% at $q_T \sim 15$ GeV, and it increases again to about ±15% at $q_T = 50$ GeV.

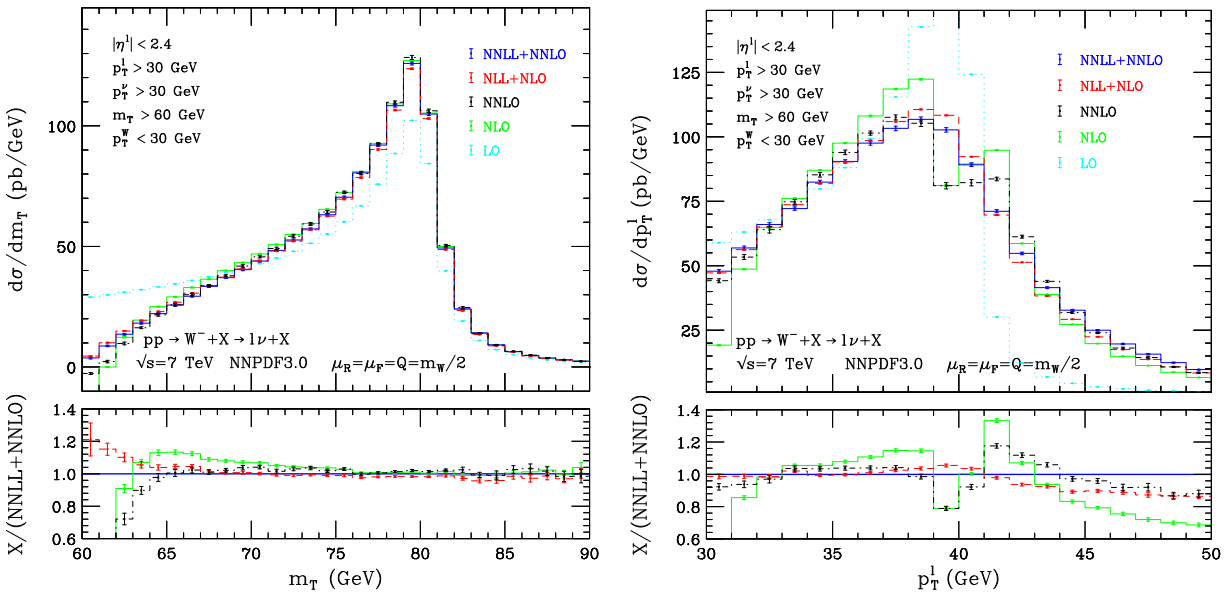

FIGURE 3. Effect of q_T resummation for $pp \to W^- \to l^-\bar{\nu}_l$ production at the LHC: (a) transverse-mass (m_T) distribution and (b) lepton p_T distribution. Comparison of results of the fixed-order calculation at LO (cyan dotted), NLO (green solid) and NNLO (black dot-dashed) with the resummed calculation at NLL+NLO (red dashed) and NNLL+NNLO (blue solid) accuracy. The lower panel shows the ratio between the various results (excluding the LO result) and the NNLL+NNLO result.

We finally study the impact of q_T resummation on some kinematical distributions that are relevant for the measurement of the W mass. We consider $pp \to W^- \to l^-\bar{\nu}_l$ with $\sqrt{s} = 7$ TeV and we apply the following selection cuts: the charged lepton has transverse momentum $p_T^l > 30$ GeV and rapidity $|\eta^l| < 2.4$, the missing transverse momentum is $p_T^\nu > 30$ GeV, and the transverse mass is $m_T > 60$ GeV. We also apply a cut on the transverse momentum p_T^W of the

W boson, $p_T^W < 30$ GeV. The results of our calculation of the m_T distribution and of the lepton momentum distributions are presented in Fig. 3. The reference scale choice of the calculation is $\mu_F = \mu_R = Q = m_W/2$. We present the results of the fixed-order calculation at LO (cyan dotted), NLO (green solid) and NNLO (black dot-dashed) accuracy and we compare them with the results of the q_T resummed calculation at NLL+NLO (red dashed) and NNLL+NNLO (blue solid) accuracy. The lower panel shows the ratio between the various results (excluding the LO result) and the NNLL+NNLO result.

The m_T distribution in the range $m_T < 90$ GeV is presented in Fig. 3 (a). We can consider two regions: the large-m_T region, around $m_T \sim m_W$ and the small-m_T region. In the large-m_T region, we see that the perturbative prediction is extremely stable against radiative corrections. This is a consequence of the well known fact that the transverse mass is weakly sensitive to the transverse momentum of the W boson. On the contrary, in the small-m_T region, we observe that the fixed-order predictions become unreliable. This is due to the fact that the kinematical constraints $p_T^l > 30$ GeV and $p_T^\nu > 30$ GeV produce an unphysical boundary (and a stepwise behaviour) of the m_T distribution at $m_T = 60$ GeV in the LO calculation. The boundary is due to the LO kinematics ($q_T = 0$) and it disappears at higher orders. The LO boundary induces (integrable) logarithmic singularities [43] which are resummed to all order by q_T resummation, and the the resummed prediction is well behaved at the LO boundary.

In Fig. 3 (b) we present the p_T^l distribution. In the limit in which the W boson is produced on shell, this distribution has an LO kinematical boundary at $m_W/2$. The finite width of the W boson (partially) smears this effect: at LO both the p_T^l and p_T^ν distributions are strongly peaked at $m_W/2$ (Jacobian peak) and quickly drop for $p_T \gtrsim m_W/2$. The almost stepwise behaviour of the LO distribution produces large radiative corrections at NLO and beyond [43]. The NLO and NNLO distributions indeed display an unphysical peak at $p_T \sim 42$ GeV, which is an artifact of such large corrections. The resummed predictions at NLL+NLO and NNLL+NNLO accuracy are free of such instabilities and display a smooth *shoulder* behaviour around the LO boundary for on-shell production. The perturbative instabilities of the fixed-order calculation at small values of p_T are analogous to those that we have previously discussed in the case of the m_T distribution in the region $m_T \sim 60$ GeV. The resummed calculation is perturbatively stable in the small-p_T region, and the differences between the NLL+NLO and NNLL+NNLO results are small throughout the entire region with $p_T \lesssim 45$ GeV. In the large-p_T region ($p_T \gtrsim 45$ GeV) the NLO calculation is essentially the first perturbative order at which both the p_T^l distribution is non vanishing and therefore in this region the p_T^l distribution display relatively large radiative corrections.

Summary

We have presented the calculation of the transverse-momentum (q_T) distribution of Drell–Yan high-mass lepton pairs performed in Ref. [28], which is based on the transverse-momentum resummation formalism developed in Refs. [21, 22, 23]. We have performed a perturbative QCD study up to next-to-next-to-leading logarithmic (NNLL) accuracy, combining small-q_T resummation with the complete $O(\alpha_S^2)$ fixed-order result at small, intermediate and large values of q_T. In particular, the calculation exactly reproduces the complete NNLO total cross section after integration over q_T. This leads to theoretical predictions with a controllable and uniform perturbative accuracy over the region from small up to large values of q_T.

In the case of vector boson production at LHC energies, we have estimated the theoretical uncertainties due to uncalculated higher-order QCD corrections by performing a systematic study on factorization, renormalization and resummation scale dependence with the `DYqT` code [26, 27].

We have explicitly included the leptonic decay of the Z/γ^* and W vector bosons with the corresponding spin correlations, the finite-width effects and the full dependence on the final-state leptonic variables, and we have consistently treated in the resummation procedure the q_T recoil due to the transverse momentum of the vector boson.

We have compared our resummed results for Z/γ^* and W production with some of the available LHC data applying the same kinematical cuts on final state leptons that are considered in the experimental analyses. We find that the data are well described by our predictions within the perturbative uncertainties. We have also considered the impact of transverse-momentum resummation on observable, which are different from the vector boson q_T, that depend on the lepton kinematical variables, such as the leptonic transverse-momentum, and the transverse-mass distributions in W production.

Our calculation is implemented in the publicly available parton-level Monte Carlo numerical code `DYRes` which allows the user to apply arbitrary kinematical cuts on the vector boson and the final-state leptons, and to compute the corresponding relevant distributions in the form of bin histograms.

REFERENCES

[1] S. D. Drell and T. M. Yan, Phys. Rev. Lett. **25** (1970) 316 [Erratum-ibid. **25** (1970) 902].
[2] R. Hamberg, W. L. van Neerven and T. Matsuura, Nucl. Phys. B **359** (1991) 343 [Erratum-ibid. B **644** (2002) 403]; R. V. Harlander and W. B. Kilgore, Phys. Rev. Lett. **88** (2002) 201801.
[3] C. Anastasiou, L. J. Dixon, K. Melnikov and F. Petriello, Phys. Rev. D **69** (2004) 094008.
[4] K. Melnikov and F. Petriello, Phys. Rev. Lett. **96** (2006) 231803, Phys. Rev. D **74** (2006) 114017; R. Gavin, Y. Li, F. Petriello and S. Quackenbush, Comput. Phys. Commun. **182** (2011) 2388.
[5] S. Catani, L. Cieri, G. Ferrera, D. de Florian and M. Grazzini, Phys. Rev. Lett. **103** (2009) 082001.
[6] S. Catani, G. Ferrera and M. Grazzini, JHEP **1005** (2010) 006.
[7] S. Dittmaier and M. Kramer, Phys. Rev. D **65** (2002) 073007; U. Baur and D. Wackeroth, Phys. Rev. D **70** (2004) 073015; V. A. Zykunov, Phys. Atom. Nucl. **69** (2006) 1522 [Yad. Fiz. **69** (2006) 1557]; A. Arbuzov et al., Eur. Phys. J. C **46** (2006) 407 [Erratum-ibid. C **50** (2007) 505]; C. M. Carloni Calame, G. Montagna, O. Nicrosini and A. Vicini, JHEP **0612** (2006) 016; U. Baur, O. Brein, W. Hollik, C. Schappacher and D. Wackeroth, Phys. Rev. D **65** (2002) 033007; V. A. Zykunov, Phys. Rev. D **75** (2007) 073019; C. M. Carloni Calame, G. Montagna, O. Nicrosini and A. Vicini, JHEP **0710** (2007) 109; A. Arbuzov et al., Eur. Phys. J. C **54** (2008) 451.
[8] A. Kotikov, J. H. Kuhn and O. Veretin, Nucl. Phys. B **788** (2008) 47; W. B. Kilgore and C. Sturm, Phys. Rev. D **85** (2012) 033005; R. Bonciani, PoS EPS **-HEP2011** (2011) 365; S. Dittmaier, A. Huss and C. Schwinn, Nucl. Phys. B **885** (2014) 318.
[9] R. K. Ellis, G. Martinelli and R. Petronzio, Nucl. Phys. B **211** (1983) 106.
[10] P. B. Arnold and M. H. Reno, Nucl. Phys. B **319** (1989) 37 [Erratum-ibid. B **330** (1990) 284].
[11] R. J. Gonsalves, J. Pawlowski and C. F. Wai, Phys. Rev. D **40** (1989) 2245.
[12] E. Mirkes, Nucl. Phys. B **387** (1992) 3.
[13] E. Mirkes and J. Ohnemus, Phys. Rev. D **51**, 4891 (1995).
[14] R. Boughezal, C. Focke, X. Liu and F. Petriello, Phys. Rev. Lett. **115** (2015) 6, 062002 doi:10.1103/PhysRevLett.115.062002.
[15] A. G. D. Ridder, T. Gehrmann, E. W. N. Glover, A. Huss and T. A. Morgan, arXiv:1507.02850 [hep-ph].
[16] Y. L. Dokshitzer, D. Diakonov and S. I. Troian, Phys. Lett. B **79** (1978) 269, Phys. Rep. **58** (1980) 269; G. Parisi and R. Petronzio, Nucl. Phys. B **154** (1979) 427; G. Curci, M. Greco and Y. Srivastava, Nucl. Phys. B **159** (1979) 451.
[17] J. C. Collins and D. E. Soper, Nucl. Phys. B **193** (1981) 381 [Erratum-ibid. B **213** (1983) 545].
[18] J. C. Collins and D. E. Soper, Nucl. Phys. B **197** (1982) 446.
[19] J. C. Collins, D. E. Soper and G. Sterman, Nucl. Phys. B **250** (1985) 199.
[20] J. Kodaira and L. Trentadue, Phys. Lett. B **112** (1982) 66, report SLAC-PUB-2934 (1982), Phys. Lett. B **123** (1983) 335.
[21] S. Catani, D. de Florian and M. Grazzini, Nucl. Phys. B **596** (2001) 299.
[22] G. Bozzi, S. Catani, D. de Florian and M. Grazzini, Nucl. Phys. B **737** (2006) 73.
[23] G. Bozzi, S. Catani, D. de Florian and M. Grazzini, Nucl. Phys. B **791** (2008) 1.
[24] S. Catani and M. Grazzini, Nucl. Phys. B **845** (2011) 297.
[25] S. Catani, L. Cieri, D. de Florian, G. Ferrera and M. Grazzini, Nucl. Phys. B **881** (2014) 414.
[26] G. Bozzi, S. Catani, G. Ferrera, D. de Florian and M. Grazzini, Nucl. Phys. B **815** (2009) 174.
[27] G. Bozzi, S. Catani, G. Ferrera, D. de Florian and M. Grazzini, Phys. Lett. B **696** (2011) 207.
[28] S. Catani, D. de Florian, G. Ferrera and M. Grazzini, JHEP **1512** (2015) 047.
[29] S. Catani, L. Cieri, D. de Florian, G. Ferrera and M. Grazzini, Eur. Phys. J. C **72** (2012) 2195.
[30] S. Catani, E. D'Emilio and L. Trentadue, Phys. Lett. B **211** (1988) 335.
[31] D. de Florian and M. Grazzini, Phys. Rev. Lett. **85** (2000) 4678, Nucl. Phys. B **616** (2001) 247.
[32] S. Catani and M. Grazzini, Eur. Phys. J. C **72** (2012) 2013 [Eur. Phys. J. C **72** (2012) 2132].
[33] T. Gehrmann, T. Luebbert and L. L. Yang, JHEP **1406** (2014) 155.
[34] S. Catani and M. Grazzini, Phys. Rev. Lett. **98** (2007) 222002.
[35] D. de Florian, G. Ferrera, M. Grazzini and D. Tommasini, JHEP **1111** (2011) 064, JHEP **1206** (2012) 132.
[36] L. Cieri, F. Coradeschi and D. de Florian, JHEP **1506** (2015) 185; M. Grazzini, S. Kallweit, D. Rathlev and M. Wiesemann, JHEP **1508** (2015) 154.
[37] R. D. Ball *et al.* [NNPDF Collaboration], JHEP **1504** (2015) 040.
[38] K. A. Olive *et al.* [Particle Data Group Collaboration], Chin. Phys. C **38** (2014) 090001.
[39] G. Bozzi, S. Catani, D. de Florian and M. Grazzini, Phys. Lett. B **564** (2003) 65.
[40] G. Aad *et al.* [ATLAS Collaboration], JHEP **1409** (2014) 145.
[41] S. Chatrchyan *et al.* [CMS Collaboration], Phys. Rev. D **85** (2012) 032002.
[42] G. Aad *et al.* [ATLAS Collaboration], Phys. Rev. D **85** (2012) 012005.
[43] S. Catani and B. R. Webber, JHEP **9710** (1997) 005.

Proceedings of the LHCP2015 Conference, St. Petersburg, Russia, August 31 - September 5, 2015

Editors: V.T. Kim and D.E. Sosnov

Measurements of Single Electroweak Boson Production in 13 TeV pp Collisions with the ATLAS Detector

JASON NIELSEN

Santa Cruz Institute for Particle Physics, University of California, Santa Cruz 95064 U.S.A.

On behalf of the ATLAS Collaboration

Abstract. The $W \to \ell\nu$ and $Z \to \ell^+\ell^-$ production cross sections have been measured in pp collisions at 13 TeV using 85 pb^{-1} of data recorded with the ATLAS experiment at the LHC. Results are presented for the total cross section and for the cross section in a restricted fiducial phase space. The total inclusive $W^{\pm}$ cross section times single-flavor lepton branching ratio is 19350 ± 20 (stat.) ± 760 (syst.) ± 1740 (lumi.) pb, and the total inclusive Z cross section times leptonic branching ratio is 1869 ± 7(stat.)±42(syst.)±(lumi.) pb. Theoretical predictions of W and Z production, using different PDF sets and Monte Carlo generators, are compared to the ATLAS measurements at 13 TeV.

INTRODUCTION

Measurements of electroweak boson production in hadron-hadron collisions provide a benchmark for our understanding of electroweak (EW) interactions and quantum chromodynamics (QCD). The large cross sections and clean experimental signatures make these measurements a precision test of the Standard Model. Recent calculations include contributions at NNLO in QCD with NLO EW corrections. The measurements at $\sqrt{s} = 13$ TeV represent deep probes into the proton structure and can be used to constrain parton distribution functions at low-x and high Q^2. Ratios of the production cross sections feature reduced experimental uncertainties and offer even more precise comparisons with higher-order calculations.

The cross section for W boson production and decay to a single lepton flavor can be written as

$$\sigma^{\text{tot}}_{W^{\pm}} = \sigma_W \cdot BR(W \to \ell\nu) = \frac{N^{\text{sig}}_W}{A_W \cdot C_W \cdot \mathcal{L}} \tag{1}$$

and similarly for the Z cross section. In this equation, N^{sig}_W represents the number of data events after background subtraction, A_W represents the geometric and kinematic acceptance factor, and C_W represents the correction factor due to experimental efficiencies. The corresponding W fiducial cross section is defined as

$$\sigma^{\text{fid}}_{W^{\pm}} = \sigma^{\text{tot}}_{W^{\pm}} \cdot A_W = \frac{N^{\text{sig}}_W}{C_W \cdot \mathcal{L}} \tag{2}$$

with a similar equation for the Z cross section. The acceptance factors and correction factors are calculated with dedicated Monte Carlo calculations.

The ATLAS experiment [1] collected high-quality data from pp collisions at $\sqrt{s} = 13$ TeV, corresponding to an integrated luminosity of 85 pb^{-1} during June-July 2015. During that period, the LHC circulated 6.5 TeV proton beams with 50 ns bunch spacing. The mean number of additional pp interactions per bunch crossing (pileup) was $\langle\mu\rangle = 19$. The relative uncertainty on the integrated luminosity is estimated to be 9%, using the method described in Ref. [2].

The data are compared to distributions generated with Monte Carlo simulations. Nearly all of the expected distributions were generated with the Powheg-Box v2 Monte Carlo program [3], specifically the codes for single boson production [4], interfaced with the Pythia v.8.186 parton shower program [5]. The programs used the CT10